A High-Power Dual-Transformer-Based Dual Active Bridge Converter Suitable for Electric Vehicles

Milad Babalou
Dept. Electrical Engineering
Shahid Beheshti University
Tehran, Iran
m_babalou@sbu.ac.ir

Hossein Torkaman
Dept. Electrical Engineering
Shahid Beheshti University
Tehran, Iran
h_torkaman@sbu.ac.ir

Edris Pouresmaeil
Dept. Electrical Engineering and Automation
Aalto University
Espoo, Finland
edris.pouresmaeil@aalto.fi

***Abstract*—In this paper, a dual active bridge converter based on the utilization of two transformers is presented. Also, the principles of operation, switching strategy, and transmission power characteristics of the proposed converter are discussed. Moreover, the RMS current of two transformers with different values of inductances of the inductors that are in series with the transformers; is discussed. In addition, the loss distribution of the proposed converter in different powers is investigated. The proposed dual-transformer-based dual active bridge converter is compared with the presented converters in terms of transmission power of transformers and efficiency of the converters. Finally, the proposed converter with a low voltage side (V_L= 200 V), the switching frequency of power MOSFETs (f_s= 25 kHz), and an accurate model of the electric battery at a high voltage side (V_H= 400 V) are simulated in 2980 W to verify the way of charging and discharging the electrical battery with the proposed converter.**

Keywords—dual active bridge converter, dual-transformer-based, high power, electric vehicles.

I. Introduction

Electronic power converters play a significant role in power transmission as an interface [1-3]. Bidirectional dc-dc converters are predominantly employed in energy storage systems especially in battery electric vehicles (BEV) [4-6]. Among the category of bi-directional dc-dc converters, the dual active bridge converter (DAB), which firstly was presented in [7], is a suitable candidate for this application as shown in Fig.1 [8, 9]. The reasons for this choice can be mentioned as simple and symmetrical structure, soft switching of power switches under ZVS, isolation by using a high-frequency transformer in its structure, high power density, and bi-directional transmission capability.

For DAB converter, different switching strategies have been introduced by researchers in recent years, including SPS, DPS, and TPS [10]. Also, different types of DAB converter structures have been proposed. From the point of view of sources, this converter is divided into two categories current source and voltage source. Some of the presented converters of voltage source are full-bridge and half-bridge conventional dual active bridge converters. In [11], a dual active bridge current source converter is presented, which is suitable for use in high current and low voltage applications due to the continuity of the input current of the converter by using the inductor on the input side and also the soft switching under zero current (ZCS). Moreover, the Dual active bridge converters are divided into two categories, two-level and

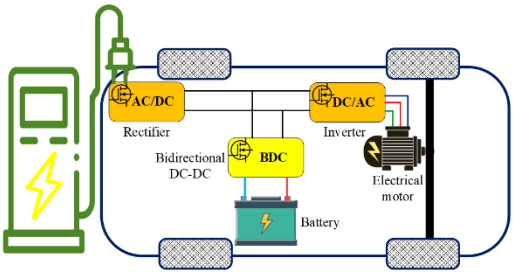

***Fig. 1**. Application of DAB converter in electric vehicles.*

multi-level, from the point of view of the input and output voltage level of its transformer. The multi-level structure of dual-active bridge converters is utilized to reduce the voltage stress of semiconductors [12]. Other types of DAB converters have been proposed, which in their structure comprise a resonant tank LC, LLC, CLLC, etc. [13]. The soft switching feature of these converters increase the frequency functional area, and, as a result, the power density.

There is another classification for DAB converters from the point of the number of transformers, Single-transformer, dual-transformer, or multi-transformer DAB converters. Dual-transformer-based DAB converters are used to reduce power stress on high-frequency transformers. In this way, a smaller transformer core is utilized compared to its single transformer-based, and as a result, the power density is somewhat improved. In [14], a dual-transformer-based DAB converter has been introduced, which has significantly reduced conduction and switching losses using the unified segmental control strategy. A dual-transformer-based DAB converter using a blocking capacitor to expand the ZVS switching range of power semiconductors is proposed in [15]. The mentioned dual-transformer-based DAB converters are not able to transmit more power at high efficiency due to the way the transformers are connected. Therefore, in this paper, a dual-transformer-based DAB converter is proposed which have the ability of high power transmission and high efficiency.

This paper consists of eight sections. In the second section, the operation principles of the proposed converter are discussed. Then, the power characteristic of the proposed DAB converter is analyzed. In the fourth section, the RMS current of the transformers is obtained. The distribution analysis of the proposed DAB converter losses is calculated in the fifth section. In the next section, the proposed converter is compared with other DAB converters. In the end, the proposed converter is simulated in PLECS software.

II. Description of the Operational Principles of the Proposed Converter

A. *The Main Structure of The Proposed Dual-Transformer DAB Converter*

The proposed DAB converter is based on a dual-transformer structure, whose equivalent circuit is depicted in Fig. 2. The proposed topology has 6 (Q_{p1}, Q_{p2}; Q_{p3}, Q_{p4}, Q_{p5} and Q_{p6}) and 4 (Q_{s1}, Q_{s2}, Q_{s3} and Q_{s4}) power switches at the low and high-voltage sides, respectively. Also, the converter has two high-frequency transformers Tr_1 and Tr_2 with the ratio of turns N_1 and N_2, respectively. Inductors L_1 and L_2 are equivalent to the sum total of the leakage inductance of the transformer with an additional inductor. On the high voltage side of the proposed topology, two electrolytic capacitors C_{H1} and C_{H2} are implemented. In contrast, the low-voltage side has an electrolytic capacitor (C_L).

B. *Operating Modes of The Proposed Dual-Transformer-Based DAB Converter*

The switching strategy of power MOSFETs as well as the voltage and current waveforms of inductors L_1 and L_2 are depicted in Fig. 3. The power MOSFETs Q_{p6}, Q_{s2}, and Q_{s3} are turned on with a phase shift φ relative to the MOSFETs Q_{p1} and Q_{p4}. It should be noted that the MOSFETs in the same leg should not be turned on at the same time. As it can be concluded from the current waveforms of the inductors shown in Fig. 3, the proposed converter has eight working modes, whose equivalent circuits are illustrated in Fig. 4, which will be discussed further.

Stage I [*Fig. 4(a)*]: At the beginning of this interval, the commands to turn on the power switches Q_{p1} and Q_{p4} are sent to their respective gates. Moreover, anti-parallel diodes of MOSFETs Q_{p1}, Q_{p4}, Q_{p5}, Q_{s1} and Q_{s4} are conducted. This time interval completes when i_{L1} reaches its zero value.

$$i_{L1}(t)=i_{L1}(t_0)+\frac{N_1 \cdot V_H+V_L}{L_1}(t-t_0) \tag{1}$$

$$i_{L2}(t)=i_{L2}(t_0)-\frac{(N_2 \cdot V_H/2)+V_L}{L_2}(t-t_0) \tag{2}$$

Stage II [*Fig. 4(b)*]: MOSFET Q_{p5}, Q_{s1} and Q_{s4} turns on with ZVS and the end of this intermission is when i_{L2} attains zero.

Stage III [*Fig. 4(c)*]: When the inductor current of L_2 reaches zero, the power switches Q_{p1} and Q_{p4} are conducted under ZVS conditions. This period ends when the Q_{p5}, Q_{s1} and Q_{s4} is turned off.

Stage IV [*Fig. 4(d)*]: At the beginning of this period, the anti-parallel diode of Q_{p6} on the primary side and Q_{s2} and Q_{s3} on the secondary side conduct. In addition, Q_{p1} and Q_{p4} are still on.

$$i_{L1}(t)=i_{L1}(t_3)-\frac{N_1 \cdot V_H}{L_1}(t-t_3) \tag{3}$$

$$i_{L2}(t)=i_{L2}(t_3)+\frac{(N_2 \cdot V_H/2)-V_L}{L_2}(t-t_3) \tag{4}$$

Stage V [*Fig. 4(e)*]: When the switches Q_{p1} and Q_{p4} are turned off, the anti-parallel diode of MOSFETs Q_{p2} and Q_{p3} conduct. This mode ends when the i_{L1} reaches zero.

$$i_{L1}(t)=i_{L1}(t_4)-\frac{N_1 \cdot V_H+V_L}{L_1}(t-t_4) \tag{5}$$

$$i_{L2}(t)=i_{L2}(t_4)+\frac{(N_2 \cdot V_H/2)+V_L}{L_2}(t-t_4) \tag{6}$$

Stage VI [*Fig. 4(f)*]: Power switches Q_{p6}, Q_{s2} and Q_{s3} turn with ZVS. At the end of this intermission, the current of i_{L2} attains zero.

Stage VII [*Fig. 4(g)*]: Power switches Q_{p2} and Q_{p3} turn on under ZVS. When the gate pulses sent related to MOSFETs Q_{p6}, Q_{s2} and Q_{s3} are turned off, this period ends.

Stage VIII [*Fig. 4(h)*]: By sending turn-on pulses to the gate of Q_{p5}, Q_{s1} and Q_{s4}, this interval starts, which directs their anti-parallel diodes.

$$i_{L1}(t)=i_{L1}(t_7)+\frac{N_1 \cdot V_H}{L_1}(t-t_7) \tag{7}$$

$$i_{L2}(t)=i_{L2}(t_7)-\frac{(N_2 \cdot V_H/2)-V_L}{L_2}(t-t_7) \tag{8}$$

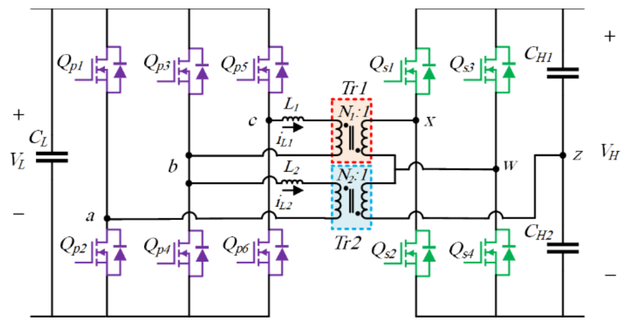

Fig. 2. The proposed dual transformer-based DAB.

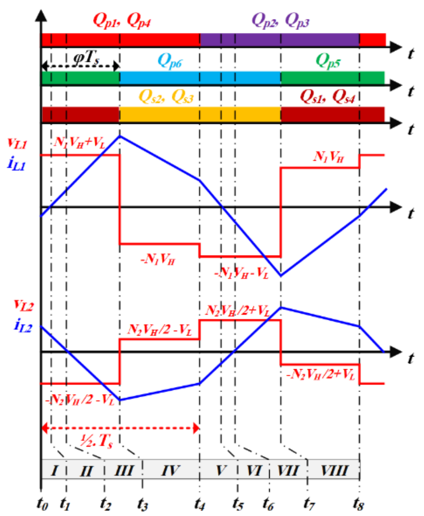

Fig. 3. Waveforms of the proposed DAB converter.

III. Analysis of Transmission Power of DAB Converter Based on Dual-Transformer

In this part, the transmission power of each of the proposed converter transformers is considered. By equating $i_{L1}(t_0)$ and $i_{L1}(t_8)$ for the L_1, and also $i_{L2}(t_0)$ and $i_{L2}(t_8)$ for the L_2, the initial value of the current of the inductors in a steady state will be obtained:

$$i_{L1}(t_0)=\frac{\left(\frac{2}{f_s}-1\right)\left(2|\varphi|V_L-N_1V_H+4|\varphi|N_1V_H\right)}{4L_1f_s} \tag{9}$$

$$i_{L2}(t_0)=-\frac{\left(\frac{2}{f_s}-1\right)\left(2V_L-N_2V_H+4|\varphi|N_2V_H\right)}{8L_2f_s} \tag{10}$$

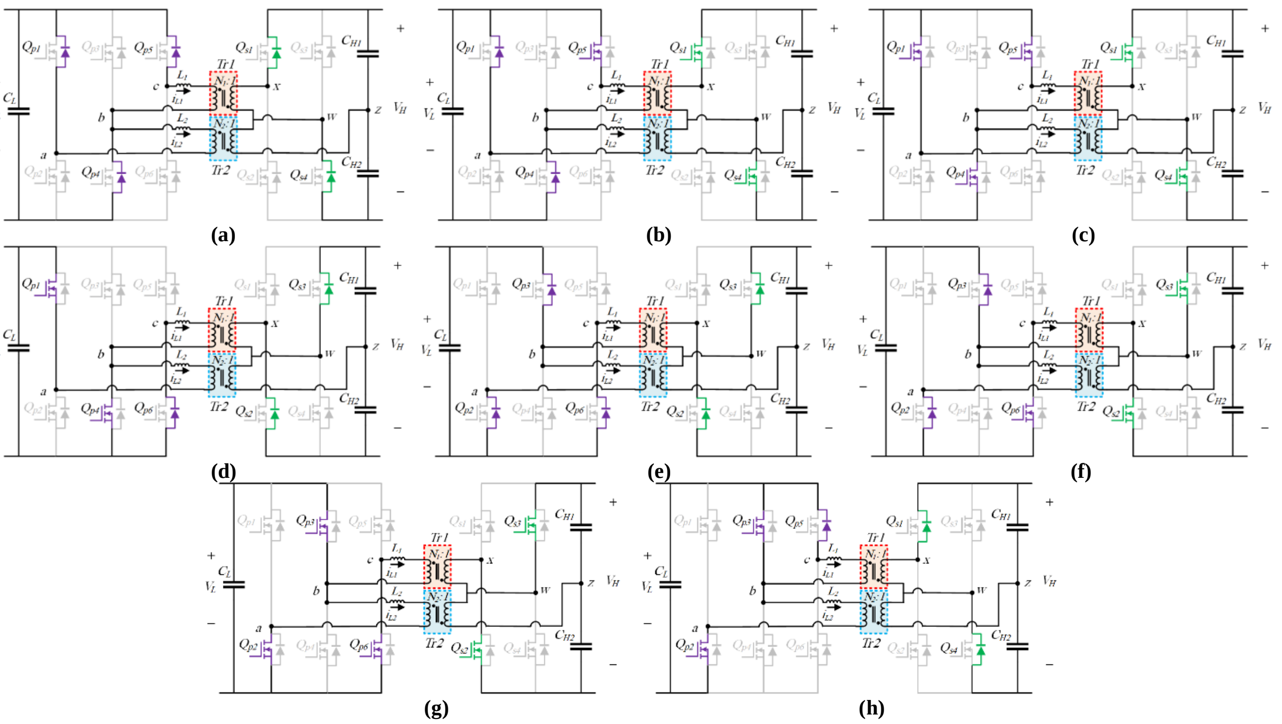

Fig. 4. *Operation principles of the proposed dual-transformer-based DAB converter;* ***(a)*** *stage I [t_0, t_1];* ***(b)*** *stage II [t_1, t_2];* ***(c)*** *stage III [t_2, t_3];* ***(d)*** *stage IV [t_3, t_4];* ***(e)*** *stage V [t_4, t_5];* ***(f)*** *stage VI [t_5, t_6];* ***(g)*** *stage VII [t_6, t_7];* ***(h)*** *stage [t_7, t_8].*

Transfer power from transformer Tr_1 is derived from:

$$P_{Tr1} = \int_0^{T_s} i_{L1}(t) \cdot v_{cb}(t)\, dt \tag{11}$$

Therefore, P_{Tr1} will be written as follows:

$$P_{Tr1} = \frac{\left[\varphi\left(1-2|\varphi|\right) N_1 V_H V_L\right]}{2 L_1 f_s} \tag{12}$$

Also, the transmission power of the transformer Tr_2 is obtained from (13), which can be written as (14):

$$P_{Tr2} = \int_0^{T_s} i_{L2}(t) \cdot v_{ba}(t)\, dt \tag{13}$$

$$P_{Tr2} = \frac{\left[\varphi\left(1-2|\varphi|\right) N_2 V_H V_L\right]}{2 L_2 f_s} \tag{14}$$

The total transmission power will be the sum of the transmission powers of these two transformers:

$$P_{Ttotal} = P_{Tr1} + P_{Tr2}$$

From (12) and (14), we can notice that if ($N_1/L_1 = N_2/L_2 = N/L$) satisfied, P_{Ttotal} can be concluded as follows:

$$P_{Ttotal} = \frac{\left[\varphi\left(1-2|\varphi|\right) N V_H V_L\right]}{L f_s} \tag{15}$$

The power characteristic curve of the proposed dual-transformer-based DAB converter in terms of p.u. for different phase shifts is illustrated in fig. 5. It should be noted that the basic power relationship is as follows:

$$P_{Base} = \frac{N V_H V_L}{8L f_s} \tag{16}$$

IV. Analysis of the RMS Current of Transformers

One of the important factors in the design of the transformer is the RMS current of its, which is discussed in this section. The RMS current at each transformer may be obtained as (18) and (19), and their corresponding coefficients are given in Table I. Also, in Fig. 6, the results related to the RMS current of each of the transformers are shown in terms of p.u. . If the ratio (N_1/L_1) is equal to (N/L), the maximum RMS current passing through the transformer Tr_1 will be 54% more than the base current, and if this ratio (N_1/L_1) is reduced to half, the maximum RMS current passing through the two transformers will be equal.

$$I_{Base} = \frac{N V_H}{8L f_s} \tag{17}$$

$$I_{L1,rms} = \sqrt{\frac{\alpha_1 N_1^2 V_H^2 + \beta_1 N_1 V_H V_L + \gamma_1 V_L^2}{48 \cdot L_1^2 f_s^2}} \tag{18}$$

$$I_{L2,rms} = \sqrt{\frac{\alpha_2 N_2^2 V_H^2 + \beta_2 N_2 V_H V_L + \gamma_2 V_L^2}{192 \cdot L_2^2 f_s^2}} \tag{19}$$

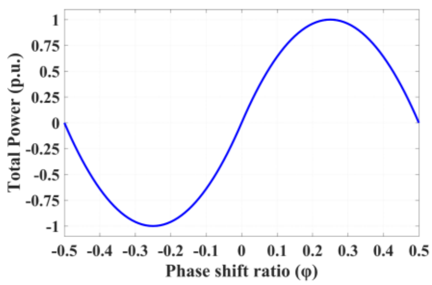

Fig. 5. *Power curve characteristic of the proposed dual-transformer-based DAB converter*

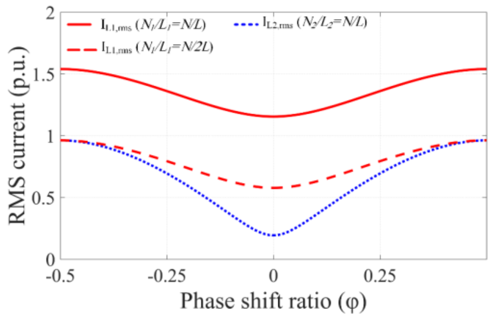

Fig. 6. The RMS current curve of transformers.

TABLE I. COEFFICIENTS RELATED TO THE RMS CURRENT OF TRANSFORMERS

RMS current	Coefficients	Equation
$I_{L1,rms}$	α_1	$192\varphi^2 T_s^2 - 96\varphi T_s^2 + 12T_s^2 + 1$
	β_1	$192\varphi^2 T_s^2 - 48\varphi T_s^2 - 32\varphi^3 + 24\varphi^2$
	γ_1	$48\varphi^2 T_s^2 - 16\varphi^3 + 12\varphi^2$
$I_{L2,rms}$	α_2	$192\varphi^2 T_s^2 - 96\varphi T_s^2 + 12T_s^2 + 1$
	β_2	$192\varphi T_s^2 - 48T_s^2 - 128\varphi^3 + 96\varphi^2 - 4$
	γ_2	$48T_s^2 + 4$

V. ANALYZING THE LOSS DISTRIBUTION IN THE PROPOSED DUAL-TRANSFORMER-BASED DAB CONVERTER

In this section, the losses of the proposed converter with specifications V_H=400 V, V_L= 200 V, f_s=25 kHz, N_1=N_2= 1.5, and L_1=L_2=200 µH in 2980 W and 2000 W, respectively, are calculated (r_{DSON}= 23 mΩ, r_L= 2.2 mΩ, r_C= 10 mΩ). The distribution of the proposed converter losses in the powers as mentioned above is depicted in Fig. 7. These losses include conduction and switching losses of power MOSFETs, iron and copper losses of transformers and inductors, and losses related to electrolytic capacitors. As shown in Fig. 7, the highest and lowest losses pertain to conduction and switching losses of power MOSFETs, respectively.

VI. COMPARISON OF THE PROPOSED CONVERTER WITH OTHER PRESENTED DUAL-TRANSFORMER DAB CONVERTERS

In Table II, the proposed DAB converter based on dual-transformers is compared with the conventional DAB converter and the converter introduced in [15]. It should be noted that the transmission power by the proposed converter is more than the converter presented in [15] with the same number of MOSFETs, capacitors, and transformers. Moreover, the efficiency of the proposed converter in the high power and the high switching frequency is higher than the proposed DAB converter in [15]. Furthermore, the power stress on transformers in the proposed converter is reduced to half.

TABLE II. COMPARISON OF THE PROPOSED CONVERTER WITH OTHER REFERRED PRESENTED CONVERTERS

Ref.	Number of Q	Number of Tr	Number of C	P_o (p.u.)	$P_{stress,T}$	Effic. (%)
Conv. DAB	8	1	2	1	1	92 @500 W, f_s= 25 kHz
[10]	10	2	3	0.89	0.5	94 @ 240 W, f_s= 20 kHz
Prop.	10	2	3	1	0.5	95.84 @ 2980 W, f_s= 25 kHz

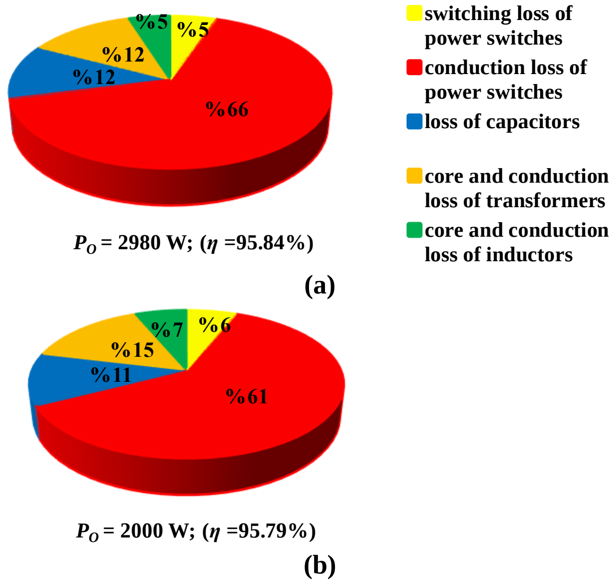

Fig. 7. Loss distribution of the proposed DAB converter under different output power; (a) 2980 W; (b) 2000 W.

VII. SIMULATION RESULTS OF THE PROPOSED DUAL-TRANSFORMER-BASED DAB CONVERTER

Specifications of the proposed DAB converter are listed in Table III and the proposed dual-transformer-based DAB is simulated in PLEXIM/PLECS software. Moreover, on the high voltage side, the accurate battery model presented in [16] with the specifications presented in Table III is implemented. Furthermore, the equivalent circuit simulated in PLECS is illustrated in Fig. 8. The proposed converter is simulated in two modes of battery charging and battery discharging, and the results are depicted in Fig. 9 and 10, which confirm the theoretical relationships obtained.

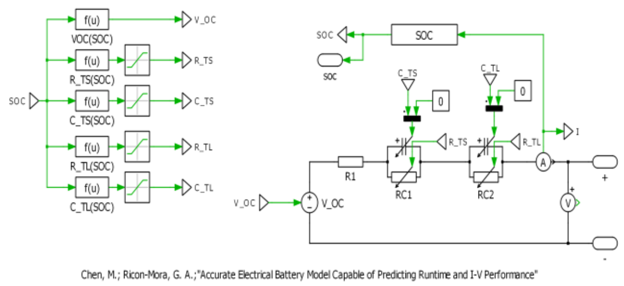

Fig. 8. The accurate battery model schematic in PLECS.

TABLE III. THE SIMULATED SPECIFICATIONS OF THE PROPOSED DUAL-TRANSFORMERS-BASED DAB CONVERTER

Devices	Properties	Value
Battery	Number of series connected cells	105
	Number of parallel branches	20
	Target constant charging voltage for each cell	4.1 V
	Target constant charging current for each cell	1.3 A
	Initial SOC	50 %
The Prop. converter	Input and output Capacitors	460 µF
	Inductors (L_1=L_2)	200 µH
	Transformers (N_1=N_2)	1.5
	Switching frequency	25 kHz
	Maximum output power	2980 W
Voltage source	Voltage	200 V

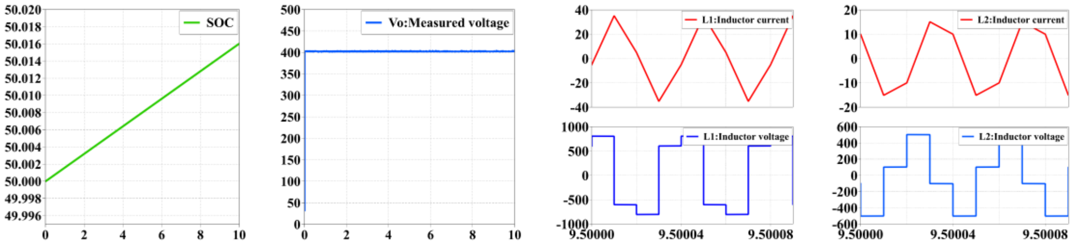

(a) (b) (c) (d)

Fig. 7. Simulation results of the proposed converter in battery charging state(φ=0.25); (a) State of Charge; (b)Output voltage; (c) current and voltage of L_1; (d) L_2.

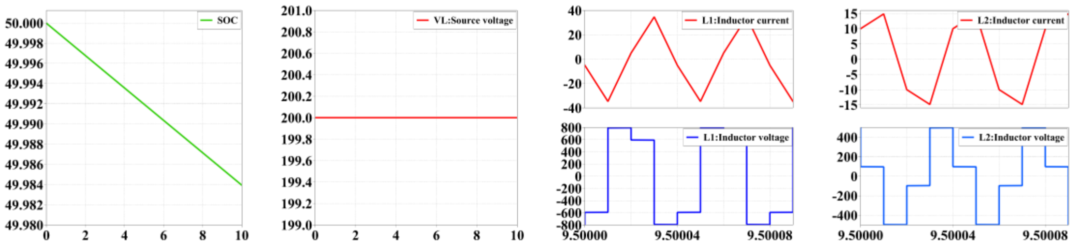

(a) (b) (c) (d)

Fig. 8. Simulation results of the proposed converter in battery discharging state(φ=-0.25); (a) State of Charge; (b)Output voltage; (c) current and voltage of L1; (d) L2.

VIII. Conclusion

In this paper, a dual-transformer-based DAB converter has been proposed. This converter has all the inherent characteristics of a DAB converter, including power MOSFETs switching in ZVS conditions and bi-directional power transmission. In addition, the proposed converter has better efficiency in high powers than one of the suggested dual-transformer-based DAB converters. Furthermore, the accurate battery model has been utilized for simulation on the high voltage side of the proposed converter in PLECS software. Eventually, the simulation results of charging and discharging the battery by the proposed converter have been validated.

Acknowledgment

This work was supported by research grants from the Iran National Science Foundation (INSF) under grant No.4005030.

References

[1] MA. Dashtaki, H. Nafisi, A. Khorsandi, M. Hojabri, E. Pouresmaeil, "Dual Two-Level Voltage Source Inverter Virtual Inertia Emulation: A Comparative Study," *Energies*. 2021; vol. 14, no. 4, pp.1160.

[2] M. Babalou, M. Dezhbord, M. Maalandish, S. H. Hosseini, M. R. Islam, and H. Torkaman, "Modular DC-DC converter with reduced current ripple and low voltage stress suitable for high voltage applications," *Int J Circ Theor Appl.*, vol. 50, no. 11, pp. 4027-4044, 2022.

[3] M. Dezhbord, M. Babalou, P. Mohseni, M. R. Islam, L. Ebrahimi Vafaei, and S. H. Hosseini, "An extendable soft-switched high step-up converter with near zero-ripple input current suitable for fuel cell-powered applications," *IET Renew. Power Gener.*, vol. 16, pp. 3287–3298, 2022.

[4] A. Sarikhani, B. Allahverdinejad, and H. Torkaman, "A non-isolated buck-boost DC-DC converter with single switch," in *9th Annual Power Electronics, Drives Systems and Technologies Conference (PEDSTC)*, Tehran, Iran, 2018, pp. 369-373.

[5] S. Khosrogorji, H. Torkaman, and F. Karimi, "A short review on multi-input DC/DC converters topologies," in *6th Power Electronics, Drive Systems & Technologies Conference (PEDSTC)*, Tehran, Iran, 2015, pp. 650-654.

[6] S. Mohammadi, M. Dezhbord, M. Babalou, M. Eskandarpour Azizkandi, and S. H. Hosseini, "A New Non-Isolated Multi-Input DC-DC Converter with High Voltage gain and Low Average of Normalized Peak Inverse Voltage," in *10th International Power Electronics, Drive Systems and Technologies Conference (PEDSTC)*, Shiraz, Iran, 2019, pp. 515-520.

[7] R. W. A. A. De Doncker, D. M. Divan, and M. H. Kheraluwala, "A three-phase soft-switched high-power-density DC/DC converter for high-power applications," *IEEE Trans. Ind. Appl.*, vol. 27, no. 1, pp. 63-73, Feb. 1991.

[8] M. R. Arabshahi, H. Torkaman, M. Bagheri, and A. Keyhani, "On the modelling, analysis, and design of a suboptimal controller for a class of wind/PV/battery based DC microgrid," *IET Renew. Power Gener.*, vol. 16, no. 2, pp. 416-434, 2022.

[9] S. A. Gorji, H. G. Sahebi, M. Ektesabi, and A. B. Rad, "Topologies and Control Schemes of Bidirectional DC–DC Power Converters: An Overview," *IEEE Access*, vol. 7, pp. 117997-118019, 2019.

[10] S. Shao, H. Chen, X. Wu, J. Zhang, and K. Sheng, "Circulating Current and ZVS-on of a Dual Active Bridge DC-DC Converter: A Review," *IEEE Access*, vol. 7, pp. 50561-50572, 2019.

[11] F. Z. Peng, H. Li, G.-J. Su, and J. S. Lawler, "A New ZVS Bidirectional DC–DC Converter for Fuel Cell and Battery Application," *IEEE Trans. Power Electron.*, vol. 19, no. 1, pp. 54-65, 2004.

[12] K. Kim and H. Cha, "Split-Capacitor Dual-Active-Bridge Converter," *IEEE Trans. Ind. Electron.*, vol. 68, no. 2, pp. 1445-1453, Feb. 2021.

[13] G. Li, D. Yang, B. Zhou, Y.-F. Liu, and H. Zhang, "Integration of Three-Phase LLC Resonant Converter and Full-Bridge Converter for Hybrid Modulated Multioutput Topology," *IEEE J. Emerg. Sel. Topics Power Electron.*, vol. 10, no. 5, pp. 5844-5856, Oct. 2022.

[14] D. Chen, J. Deng, W. Wang, and Z. Wang, "A Dual-Transformer-Based Hybrid Dual Active Bridge Converter for Plug-in Electric Vehicle Charging to Cope with Wide Load Voltages," *IEEE Trans. Ind. Electron.*, pp. 1-1, 2022.

[15] Y. Liang, X. Liu, G. Xu, and S. Yue, "A Dual-Transformer-Based Bidirectional DC–DC Converter of Using Blocking Capacitor for Wide ZVS Range," *IEEE Access*, vol. 8, pp. 170568-170578, 2020.

[16] M. C. a. G. A. Rincon-Mora, "Accurate electrical battery model capable of predicting runtime and I-V performance," *IEEE Trans. Energy Convers.*, vol. 21, no. 2, pp. 504-511, June 2006.